51st AIAA Aerospace Sciences Meeting including the New Horizons Forum and Aerospace Exposition
07 - 10 January 2013, Grapevine (Dallas/Ft. Worth Region), Texas

AIAA 2013-0638

Quasi-periodic Time Spectral Method for Aeroelastic Flutter Analysis

Nathan L. Mundis * Dimitri J. Mavriplis †

Department of Mechanical Engineering, University of Wyoming, Laramie, Wyoming 82071-3295

A recently developed quasi-periodic time spectral method is applied to the demanding problem of aeroelastic flutter. Both a standard time-implicit method and a quasi-periodic time spectral method are developed that take into account the coupling among the three fundamental aspects of computational aeroelastic calculations: unsteady flow equations, time dependent structural response to aerodynamics loads, and dynamically moving meshes. These two methods are then compared in order to demonstrate the capability of the quasi-periodic time spectral method to solve aeroelastic flutter problems. Finally, it is demonstrated that the quasi-periodic time spectral method can be used to solve aeroelastic flutter problems.

I. Introduction

For problems with strong periodic content, such as turbomachinery flows or rotorcraft aerodynamics, time-spectral methods can be used to substantially reduce the cost of computing the full time-dependent solution for a given level of accuracy. In many cases, time-spectral methods using only a small number of time instances per period can provide equivalent or superior accuracy, at substantially reduced cost, compared to traditional time domain solutions using hundreds of time steps per period .

The time spectral method, based on the use of discrete Fourier analysis, is similar to the harmonic balance method, developed by Hall[1] and McMullen,[2,3] which transforms the unsteady equations in the physical domain to a set of steady equations in the frequency domain. Gopinath[4,5] proposed to solve the time spectral equations, not in the frequency domain, but directly in the time domain by applying the time discretization operator. The time spectral method was shown to be faster than the dual-time stepping implicit methods using backwards difference time formulae for time periodic computations, such as turbomachinery flows,[2,5] oscillatory pitching airfoil/wing cases,[4,6] flapping wing,[7] helicopter rotor[8,9] and vortex shedding problems.[3]

In the recent past, the time spectral method has been proven capable of solving the coupled fluid/structure equations for the purely periodic problem of a helicopter rotor in constant speed forward flight.[8,9] Similarly, the simulation of aeroelastic flutter phenomena is computationally expensive and could benefit tremendously from the successful application of a more efficient time integration scheme. However, time spectral methods are not directly applicable to most flutter problems since these are usually not purely periodic. In previous work, we have introduced a hybrid BDF/time-spectral approach (BDFTS) which aims to simulate quasi-periodic flows with slow transients combined with relatively fast periodic content using global BDF time step sizes of the order of the period length, while making use of the properties of the time-spectral approach to capture accurate details of the periodic flow components.[10,11,12] The aeroelastic flutter problem is a coupled fluid/structural problem with strong periodic content, i.e. the pitching and plunging of the airfoil or wing, and a slow transient, i.e. increasing or decreasing amplitude of the periodic motion. These factors, coupled with the abundance of published solutions to aeroelstic flutter problems[13,14,15] make it the ideal motivation for a coupled fluid-structure, quasi-periodic time spectral method.

In the following sections we present the necessary components for solving a two-dimensional aeroelastic flutter problem using the BDFTS time discretization. We first outline the governing equations and the base solver for the aerodynamics component. We then discuss the time spectral method and subsequently the hybrid BDF/time-spectral approach for the flow solver. Next, we discuss the structural equations and how they are transformed for efficient solution. Subsequently, we discuss some of the details of solving the structural equations simultaneously with the flow equations in the time BDFTS approach. Following, we present a brief discussion of a test problem for the BDFTS

*Graduate Student, AIAA Member; email: nmundis@uwyo.edu.
†Professor, AIAA Associate Fellow; email: mavripl@uwyo.edu.

method for the Euler equations alone. Then, we solve the coupled fluid/structure equations using the standard BDF2 time-implicit method and compare these result to previously published results. Finally, BDFTS is applied to the important practical problem of aeroelastic flutter, and the results are compared to the BDF2 approach, having been validated above.

II. Theory and Methodology

A. Flow Equations and Solver

The Euler equations in conservative form can be written as:

$$\frac{\partial \mathbf{U}}{\partial t} + \nabla \cdot (\mathbf{F}(\mathbf{U}) = 0 \tag{1}$$

where $\mathbf{U}$ represents the vector of conserved quantities (mass, momentum, and energy) and $\mathbf{F}(\mathbf{U})$ represents the convective fluxes. Integrating over a (moving) control volume $\Omega(t)$, we obtain:

$$\int_{\Omega(t)} \frac{\partial \mathbf{U}}{\partial t} dV + \int_{\partial\Omega(t)} (\mathbf{F}(\mathbf{U}) \cdot \tilde{\mathbf{n}}) dS = 0 \tag{2}$$

Using the differential identity

$$\frac{\partial}{\partial t} \int_{\Omega(t)} \mathbf{U} dV = \int_{\Omega(t)} \frac{\partial \mathbf{U}}{\partial t} dV + \int_{\partial\Omega(t)} \mathbf{U}(\dot{\mathbf{x}} \cdot \tilde{\mathbf{n}}) dS \tag{3}$$

where $\dot{\mathbf{x}}$ and $\tilde{\mathbf{n}}$ are the velocity and normal of the interface $\partial\Omega(t)$, respectively, equation (2) becomes:

$$\frac{\partial}{\partial t} \int_{\Omega(t)} \mathbf{U} dV + \int_{\partial\Omega(t)} (\mathbf{F}(\mathbf{U}) - \mathbf{U}\dot{\mathbf{x}}) \cdot \tilde{\mathbf{n}} dS = 0 \tag{4}$$

Considering $\mathbf{U}$ as cell averaged quantities, these equations are discretized in space as:

$$\frac{\partial}{\partial t}(V\mathbf{U}) + \mathbf{R}(\mathbf{U}, \dot{\mathbf{x}}(\mathbf{t}), \tilde{\mathbf{n}}(\mathbf{t})) = \mathbf{0} \tag{5}$$

where $\mathbf{R}(\mathbf{U}, \dot{\mathbf{x}}, \tilde{\mathbf{n}}) = \int_{\partial\Omega(t)} (\mathbf{F}(\mathbf{U}) - \dot{\mathbf{x}}\mathbf{U}) \cdot \tilde{\mathbf{n}} dS$ represents the discrete convective fluxes in ALE form and V denotes the control volume. In the discrete form, $\dot{\mathbf{x}}(\mathbf{t})$ and $\tilde{\mathbf{n}}(\mathbf{t})$ now represent the time varying velocities and surface normals of the control-volume boundary faces.

The Euler equations are discretized by a central difference finite-volume scheme with additional matrix-based artificial dissipation on hybrid, two-dimensional meshes, which may include triangles and quadrilaterals. Second-order accuracy is achieved using a two-pass construction of the artificial dissipation operator, which corresponds to an undivided biharmonic operator. A single unifying edge-based data-structure is used in the flow solver for all types of elements. For the base solver, the time derivative in equation (5) is discretized using a second order backwards difference (BDF2) scheme, resulting in a non-linear system to be solved at each time step. The implicit solution is achieved using flexible Generalized Minimal Residual Method algorithm, with block-colored Gauss Seidel preconditioning. This choice of linear solver allows for the efficient solution of both the BDF2 time-implicit method and the BDFTS method using the full, exact Jacobian.

1. *Time Spectral Method*

If the flow is periodic in time, the variables $\mathbf{U}$ can be represented by a discrete Fourier series. The discrete Fourier transform of $\mathbf{U}$ in a period of T is given by[4]

$$\widehat{\mathbf{U}}_k = \frac{1}{N} \sum_{n=0}^{N-1} \mathbf{U}^n e^{-ik\frac{2\pi}{T}n\Delta t} \tag{6}$$

where N is the number of time intervals and $\Delta t = T/N$. The Fourier inverse transform is then given as

$$\mathbf{U}^n = \sum_{k=-\frac{N}{2}}^{\frac{N}{2}-1} \widehat{\mathbf{U}}_k e^{ik\frac{2\pi}{T}n\Delta t} \tag{7}$$

It should be noted that $\frac{N}{2}$ is an integer division operation. Also note equation (7) corresponds to a collocation approximation, i.e. the function $\mathbf{U}(t)$ is projected into the space spanned by the truncated set of complex exponential (spectral) functions, and the expansion coefficients (in this case the $\widehat{\mathbf{U}}_k$) are determined by requiring $\mathbf{U}(t)$ to be equal to its projection at N discrete locations in time, as given by equations (6) and (7).
Differentiating equation (7) in time, we obtain:

$$\frac{\partial}{\partial t}(\mathbf{U}^n) = \frac{2\pi}{T}\sum_{k=-\frac{N}{2}}^{\frac{N}{2}-1} ik\widehat{\mathbf{U}}_k e^{ik\frac{2\pi}{T}n\Delta t} \tag{8}$$

Substituting equation (6) into equation (8), we get[16,17]

$$\frac{\partial}{\partial t}(\mathbf{U}^n) = \sum_{j=0}^{N-1} d_n^j \mathbf{U}^j \tag{9}$$

where

$$d_n^j = \begin{cases} \frac{2\pi}{T}\frac{1}{2}(-1)^{n-j}cot(\frac{\pi(n-j)}{N}) & n \neq j \\ 0 & n = j \end{cases} \tag{10}$$

for an even number of time instances and

$$d_n^j = \begin{cases} \frac{2\pi}{T}\frac{1}{2}(-1)^{n-j}cosec(\frac{\pi(n-j)}{N}) & n \neq j \\ 0 & n = j \end{cases} \tag{11}$$

for an odd number of time instances. The collocation approach for solving equation (5) consists of substituting the collocation approximation for the continuous function $\mathbf{U}(t)$ given by equation (7) into equation (5), and requiring equation (5) to hold exactly at the same N discrete locations in time (i.e. multiplying (5) by the dirac delta test function $\delta(t-t^n)$ and integrating over all time), yielding:

$$\sum_{j=0}^{N-1} d_n^j V^j \mathbf{U}^j + \mathbf{R}(\mathbf{U}^\mathbf{n}, \dot{\mathbf{x}}^\mathbf{n}, \tilde{\mathbf{n}}^\mathbf{n}) = 0 \qquad n = 0,1,2,...,N-1 \tag{12}$$

This results in a system of N equations for the N time instances $\mathbf{U}^n$ which are all coupled through the summation over the time instances in the time derivative term. The spatial discretization operators remain unchanged in the time-spectral approach, with only the requirement that each spatial solution be evaluated at the appropriate temporal location. Thus, the time-spectral method may be implemented without any modifications to an existing spatial discretization, requiring only the addition of the temporal discretization coupling term, although the N time instances must be solved simultaneously due to this coupling.

2. *Hybrid BDF/Time Spectral Method*

The quasi-periodic time-spectral form is derived through the use of polynomial subtraction for quasi-periodic functions by subtracting out the non-periodic transient, which can be modeled using a polynomial basis set, and approximating the remaining purely periodic component with a spectral basis.[18] From the point of view of a collocation method, this corresponds to using a mixed spectral/polynomial basis set for the projection of the continuous solution (in the time dimension).

We proceed by splitting the quasi-periodic temporal variation of the solution into a periodic and slowly varying mean flow as:

$$\mathbf{U}(t) = \sum_{k=-\frac{N}{2}}^{\frac{N}{2}-1} \widehat{\mathbf{U}}_k e^{ik\frac{2\pi}{T}n\Delta t} + \bar{\mathbf{U}}(t) \tag{13}$$

where the slowly varying mean flow is approximated by a collocation method using a polynomial basis set as:

$$\bar{\mathbf{U}}(t) = \phi_{12}(t)\mathbf{U}^{m+1} + \phi_{11}(t)\mathbf{U}^m \tag{14}$$

for a linear variation and

$$\bar{\mathbf{U}}(t) = \phi_{23}(t)\mathbf{U}^{m+1} + \phi_{22}(t)\mathbf{U}^m + \phi_{21}(t)\mathbf{U}^{m-1} \tag{15}$$

for a quadratic variation in time. Here $\mathbf{U}^m$ and $\mathbf{U}^{m+1}$ represent discrete solution instances in time usually taken as the beginning and ending points of the considered period in the quasi-periodic motion (and $\mathbf{U}^{m-1}$ corresponds to the beginning point of the previous period). In the first case, $\phi_{12}(t)$ and $\phi_{11}(t)$ correspond to the linear interpolation functions given by:

$$\phi_{11}(t) = \frac{t^{m+1} - t}{T} \tag{16}$$

$$\phi_{12}(t) = \frac{t - t^m}{T} \tag{17}$$

with the period given as $T = t^{m+1} - t^m$. Similarly, the $\phi_{23}(t), \phi_{22}(t), \phi_{21}(t)$ are given by the corresponding quadratic interpolation functions. Note that in this case, the collocation approximation leads to the determination of the Fourier coefficients as:

$$\widehat{\mathbf{U}}_k = \frac{1}{N} \sum_{n=0}^{N-1} \tilde{\mathbf{U}}^n e^{-ik\frac{2\pi}{T}n\Delta t} \tag{18}$$

with $\tilde{\mathbf{U}}^n = \mathbf{U}^n - \bar{\mathbf{U}}^n$ defined as the remaining periodic component of the function after polynomial subtraction. Differentiating equation (13) and making use of equations (9) and (18) we obtain the following expression for the time derivative:

$$\frac{\partial}{\partial t}(\mathbf{U}^n) = \sum_{j=0}^{N-1} d_n^j \tilde{\mathbf{U}}^j + \phi'_{12}(t_n)\mathbf{U}^{m+1} + \phi'_{11}(t_n)\mathbf{U}^m \tag{19}$$

for the case of a linear polynomial functions in time. The $\phi'_{12}(t_n)$ and $\phi'_{11}(t_n)$ represent the time derivatives of the polynomial basis functions (resulting in the constant values $\frac{-1}{T}$ and $\frac{1}{T}$ in this case), and the various time instances are given by:

$$t_j = t_m + \frac{j}{N}(t_{m+1} - t_m), \qquad j = 0, \ldots, N-1$$

We also note that $\bar{\mathbf{U}}(t_m) = \mathbf{U}^m = \mathbf{U}(t_m)$ and thus we have $\tilde{\mathbf{U}}^0 = 0$. In other words, the constant mode in the spectral representation must be taken as zero, since it is contained in the polynomial component of the function representation. Therefore, the $j = 0$ component in the summation can be dropped, and rewriting equation (19) in terms of the original time instances $\mathbf{U}^n$ we obtain:

$$\frac{\partial}{\partial t}(\mathbf{U}^n) = \sum_{j=1}^{N-1} d_n^j \mathbf{U}^j - \Big(\sum_{j=1}^{N-1} d_n^j \phi_{12}(t_j) - \phi'_{12}(t_n)\Big)\mathbf{U}^{m+1} - \Big(\sum_{j=1}^{N-1} d_n^j \phi_{11}(t_j) - \phi'_{11}(t_n)\Big)\mathbf{U}^m \tag{20}$$

Finally, the above expression for the time derivative is substituted into equation (5) which is then required to hold exactly at time instances $j = 1, 2, ..., N-1$ and $j = N$ (which corresponds to the $m+1$ time instance):

$$\sum_{j=1}^{N-1} d_n^j V^j \mathbf{U}^j - \Big(\sum_{j=1}^{N-1} d_n^j \phi_{12}(t_j) - \phi'_{12}(t_n)\Big)V^{m+1}\mathbf{U}^{m+1} - \Big(\sum_{j=1}^{N-1} d_n^j \phi_{11}(t_j) - \phi'_{11}(t_n)\Big)V^m\mathbf{U}^m + \mathbf{R}(\mathbf{U}^\mathbf{n}, \dot{\mathbf{x}}^\mathbf{n}, \tilde{\mathbf{n}}^\mathbf{n}) = 0 \quad n = 1, 2, ..., N \tag{21}$$

As previously, we have N coupled equations for the N unknown time instances, although in this case the $j = 0$ time instance which corresponds to the $\mathbf{U}^m$ values are known from the solution of the previous period, while the $j = N$ or $\mathbf{U}^{m+1}$ values are not known, since these are not equal to the $j = 0$ values as they would be in a purely periodic flow. In the case of vanishing periodic content, summation terms involving the d_n^j coefficients vanish by virtue of equation (19) with $\tilde{\mathbf{U}}^j = 0$ and it is easily verified that the above formulation reduces to a first-order backwards difference scheme with a time step equal to the period T. On the other hand, for purely periodic motion, we have $\mathbf{U}^{m+1} = \mathbf{U}^m$ which results in cancellation of the polynomial derivative terms $\phi'_{12}(t_n)$ and $\phi'_{11}(t_n)$. Furthermore, using the identities $\phi_{12}(t_j) + \phi_{11}(t_j) = 1$, and $\sum_{j=0}^{N-1} d_n^j = 0$, it can be seen that the remaining polynomial terms reduce to the missing $j = 0$ instance in the summation. Given the equality $\mathbf{U}^{m+1} = \mathbf{U}^m$, the last equation at $j = N$ becomes identical to the $j = 0$ equation and the time-spectral method given by equation (12) is recovered.

In this description we have used linear polynomials corresponding to a BDF1 time-stepping scheme for clarity. In practice, BDF2 time-stepping schemes are required for accuracy purposes, and the equivalent scheme based on

quadratic polynomials is given as:

$$\sum_{j=1}^{N-1} d_n^j V^j \mathbf{U}^j - (\sum_{j=1}^{N-1} d_n^j \phi_{23}(t_j) - \phi'_{23}(t_n)) V^{m+1} \mathbf{U}^{m+1} \tag{22}$$
$$-(\sum_{j=1}^{N-1} d_n^j \phi_{22}(t_j) - \phi'_{22}(t_n)) V^m \mathbf{U}^m - (\sum_{j=1}^{N-1} d_n^j \phi_{21}(t_j) - \phi'_{21}(t_n)) V^{m-1} \mathbf{U}^{m-1}$$
$$+\mathbf{R}(\mathbf{U^n}, \dot{\mathbf{x}}^\mathbf{n}, \tilde{\mathbf{n}}^\mathbf{n}) = 0 \quad n = 1, 2, ..., N$$

where the values $\mathbf{U}^{m-1}$ and $\mathbf{U}^m$, which correspond to the time instances at the beginning and end of the previous period are known from the solution of earlier periods, and $\mathbf{U}^{m+1} = \mathbf{U}^N$ as previously.

3. BDFTS Flow Solver

Equation (22) is solved implicitly for the flow equations at each pseudo-timestep. The flow Jacobian, which couples together the flow variables in all elements of the mesh as well as between the elements of one time instance and those of the other time instances, is formed by differentiating equation (22) with respect to the flow variables. The fully coupled flow Jacobian is a $[(4xNxE)x(4xNxE)]$ matrix which must be inverted to find the flow update. N is the number of time-spectral instances and E is the number of elements in the mesh. Only the non-zero blocks of the Jacobian are computed and stored.

The flow Jacobian is inverted using a Flexible Generalized Minimal Residual method that uses a block-colored Gauss-Siedel stationary iterative method as a preconditioner. For the preconditioner, each spatial solution (time-instance) is preconditioned independently of the other time insatnces using the corresponding first-order spatial Jacobian. A specified number of iterations of the preconditioner, usually ten to thirty, are run for each Krylov vector. As many as 1024 Krylov vectors can be used in a given restart, and the FGMRES routine can restart as many as five times for each non-linear iteration. Most non-linear iterations will converge without any restarts and fewer than 200 Krylov vectors. More details of the FGMRES, BDFTS solver implementation will be given in a subsequent paper by the same authors.

B. Structural Equations and Solver

The aeroelastic model is based on the response of an airfoil with two degrees of freedom, namely pitch and plunge as shown in Figure (1).

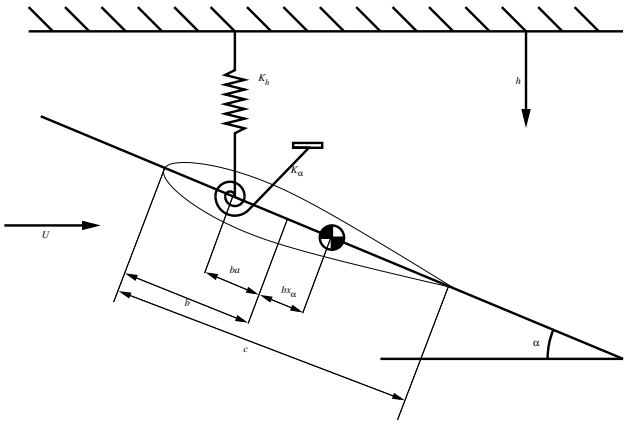

Figure 1. Two degree of freedom 2-D aeroelastic problem schematic

The equations of motion for such a system can be summarized as:

$$m\ddot{h} + S_\alpha \ddot{\alpha} + K_h h = -L \tag{23}$$
$$S_\alpha \ddot{h} + I_\alpha \ddot{\alpha} + K_\alpha \alpha = M_{ea} \tag{24}$$

where

m: mass of airfoil
S_α: static imbalance
I_α: sectional moment of inertia of airfoil
K_h: plunging spring coefficient
K_α: pitching spring coefficient
h: vertical displacement (positive downward)
α: angle-of-attack
L: sectional lift of airfoil
M_{ea}: sectional moment of airfoil about elastic axis (positive nose up)

Non-dimensionalizing time in equations (23) and (24) by the uncoupled natural frequency of pitch yields:

$$[M]\ddot{\mathbf{q}} + [K]\mathbf{q} = \mathbf{F} \tag{25}$$

where

$$[M] = \begin{bmatrix} 1 & x_\alpha \\ x_\alpha & r_\alpha^2 \end{bmatrix}, \quad [K] = \begin{bmatrix} \left(\frac{\omega_h}{\omega_\alpha}\right)^2 & 0 \\ 0 & r_\alpha^2 \end{bmatrix} \tag{26}$$

are the non-dimensional mass and stiffness matrices. The corresponding non-dimensional load and displacement vectors are:

$$\mathbf{F} = \frac{1}{\pi\mu k_c^2}\begin{bmatrix} -C_l \\ 2C_m \end{bmatrix}, \quad \mathbf{q} = \begin{bmatrix} \frac{h}{b} \\ \alpha \end{bmatrix}, \quad \ddot{\mathbf{q}} = \frac{\partial^2 \mathbf{q}}{\partial \tau^2} \tag{27}$$

where

b: semichord of airfoil
k_c: reduced frequency of pitch, $k_c = \frac{\omega_\alpha c}{2U_\infty}$
μ: airfoil mass ratio, $\mu = \frac{m}{\pi\rho b^2}$
ω_h, ω_α: uncoupled natural frequencies of plunge and pitch
x_α: structural parameter defined as $\frac{S_\alpha}{mb}$
r_α^2: structural parameter defined as $\frac{I_\alpha}{mb}$
C_l, C_m: section lift coefficient and section moment coefficient about the elastic axis
τ: structural time, $\tau = \omega_\alpha t$

The reduced frequency k_c is typically written in terms of the flutter velocity V_f as

$$k_c = \frac{\omega_\alpha c}{2U_\infty} = \frac{1}{V_f\sqrt{\mu}} \tag{28}$$

where c is the chord length of the airfoil, U_∞ is the freestream velocity, and the flutter velocity V_f is defined as

$$V_f = \frac{U_\infty}{\omega_\alpha b\sqrt{\mu}} \tag{29}$$

The natural pitch frequency is found by solving equation (29) for ω_α in terms of the prescribed flutter velocity V_f.

1. *Transformation of Structural Equations into First Order Form*

The aeroelastic equations as shown in Equation (25) are second-order partial differential equations. A transformation to first-order equations is used in order to facilitate a solution procedure for the standard BDF2 time discretization. The transformation used is:

$$\mathbf{r_1} = \mathbf{q} \tag{30}$$
$$\mathbf{r_2} = \dot{\mathbf{r}}_\mathbf{1} \tag{31}$$

The resulting first-order equations are then:

$$\dot{\breve{\mathbf{r}}}_1 = \mathbf{r}_2 \tag{32}$$

$$\dot{\breve{\mathbf{r}}}_2 = -[M]^{-1}[K]\mathbf{r}_1 + [M]^{-1}\mathbf{F} \tag{33}$$

and in matrix notation:

$$\begin{Bmatrix} \dot{\breve{\mathbf{r}}}_1 \\ \dot{\breve{\mathbf{r}}}_2 \end{Bmatrix} + \begin{bmatrix} 0 & -[I] \\ [M]^{-1}[K] & 0 \end{bmatrix} \begin{bmatrix} \mathbf{r}_1 \\ \mathbf{r}_2 \end{bmatrix} = \begin{Bmatrix} 0 \\ [M]^{-1}\mathbf{F} \end{Bmatrix} \tag{34}$$

$$\dot{\breve{\mathbf{r}}} + [\Psi]\mathbf{r} = \{\Phi\} \tag{35}$$

The matrix $[\Psi]$ is a constant and can be precomputed and stored for use during the time-integration process. The time derivative term $\dot{\breve{\mathbf{r}}}$ can be discretized using second-order (or first-order) accurate backward difference formulas similar to the time derivative term in the flow equations, as follows:

$$\frac{3\mathbf{r}^{n+1} - 4\mathbf{r}^n + \mathbf{r}^{n-1}}{2\Delta\tau} + [\Psi]\mathbf{r}^{n+1} = \{\Phi\} \tag{36}$$

or it can be discretized using BDFTS formulae, similar to equation (22), as:

$$\sum_{j=1}^{N-1} \breve{d}_n^j \mathbf{r}^j - (\sum_{j=1}^{N-1} \breve{d}_n^j \breve{\phi}_{23}(\tau_j) - \breve{\phi}'_{23}(\tau_n))\mathbf{r}^{m+1} - (\sum_{j=1}^{N-1} \breve{d}_n^j \breve{\phi}_{22}(\tau_j) - \breve{\phi}'_{22}(\tau_n))\mathbf{r}^m \tag{37}$$
$$-(\sum_{j=1}^{N-1} \breve{d}_n^j \breve{\phi}_{21}(\tau_j) - \breve{\phi}'_{21}(\tau_n))\mathbf{r}^{m-1} + [\Psi]\mathbf{r}^n = \{\Phi\} \quad n = 1,2,...,N$$

It should be noted that the time-step $\Delta\tau$ appearing in the denominator of the discretized version of the structural equations is different from the time-step of the flow equations, and their relation is $\Delta\tau = \omega_\alpha \Delta t$, where Δt is the non-dimensional time-step used for the flow equations. Similarly, the period used to calculate the $\breve{d}_n^j$ and $\breve{\phi}$ in BDFTS is the structural period. A breve ($\breve{}$) is placed above all quantities that use stuctural time for clarity.

2. *Structural Solver*

For the time-implicit approach, Equation (36) is rearranged to get the terms that are independent of the current solution on the right hand side and only the dependent terms on the left hand side, which gives the following matrix equation:

$$\left[[\Psi] + \frac{3}{2}\frac{[I]}{\Delta\tau}\right]\mathbf{r}^{n+1} = \{\Phi\} + 2\frac{\mathbf{r}^n}{\Delta\tau} - \frac{1}{2}\frac{\mathbf{r}^{n-1}}{\Delta\tau} \tag{38}$$

This matrix equation is then solved by inverting the $[4x4]$ matrix on the left hand side directly using LU-decomposition. Once the vector $\mathbf{r}^{n+1}$ at a time-level $n+1$ has been found, the displacement vector is known and the orientation of the mesh (i.e. x^{n+1}) can be computed, and the subsequent time-step can then be solved.

The solution of the BDFTS structural equations follows a similar approach. First, Equation (37) is rearranged into dependent and independent sides as:

$$\left[[\Psi]\mathbf{r}^n + \sum_{j=1}^{N-1} \breve{d}_n^j \mathbf{r}^j - (\sum_{j=1}^{N-1} \breve{d}_n^j \breve{\phi}_{23}(\tau_j) - \breve{\phi}'_{23}(\tau_n))\mathbf{r}^{m+1}\right] = \tag{39}$$
$$\{\Phi\} + (\sum_{j=1}^{N-1} \breve{d}_n^j \breve{\phi}_{22}(\tau_j) - \breve{\phi}'_{22}(\tau_n))\mathbf{r}^m + (\sum_{j=1}^{N-1} \breve{d}_n^j \breve{\phi}_{21}(\tau_j) - \breve{\phi}'_{21}(\tau_n))\mathbf{r}^{m-1} \quad n = 1,2,...,N$$

Although it may not be immediately clear, the left had side of (39) is a $[(4xN)x(4xN)]$ matrix that couples the four solution variables from each of the N time instances together with all other time instances, and the right hand side is a $\{4xN\}$ vector that couples each of the structural variables to the flow variables C_L and C_m and to the past values of the structural variables. This equation is then solved by inverting the BDFTS structral matrix on the left hand side. Although, N is generally sufficiently small that the BDFTS structural matrix could be inverted directly, it was decided to use Generalized Minimal Residual Method for the inversion so that an increase in N does not slow this step significantly. Coupling the fluid and structure equations for the BDFTS approach is more complicated than the time-implicit coupling and will be discussed in the next subsection.

3. Details of the BDFTS Aeroelastic Approach and Coupling

The most complicated aspect of solving the coupled fluid/structure equations is how to best couple the two sets of equations. For the time-implicit approach, the small time-step used allows a full coupling to be used at every pseudo-time iteration as the solution for a given time-step is solved. For the BDFTS approach, however, the much larger time-step, which is a full flutter period, precludes the possibility of such close or frequent coupling updates. For BDFTS, coupling proceeds as follows:

1. Completely solve the flow equations (22) for the current values of the structural variables $\mathbf{r}$
2. Use the flow solution to calculate lift and moment coefficients, C_L and C_m
3. Use the calculated C_L and C_m in equation (37) to find new values for $\mathbf{r}$
4. Subtract the old values of $\mathbf{r}$ from the new values to find $\Delta\mathbf{r}$
5. Add $\kappa\Delta\mathbf{r}$ to the old values of $\mathbf{r}$ to find new values of $\mathbf{r}$
6. If $\Delta\mathbf{r}$ is sufficiently small, exit and proceed to the next period; if not, go to 1 and repeat until converged

The kappa (κ) above is a structural relaxation coefficient. Values for κ between 0.05 and 0.1 have been found to be sufficient for many cases. Values below 0.05 do not appear to offer any additional advantage in terms of increased robustness and significantly lessen the convergence rate. It should also be noted that the flow solution is converged completely before the structural equations are updated. This complete convergence of the flow solution is done principally for robustness and future work will investigate more efficient strategies for solving the coupled aeroelastic system.

Another exceptional aspect of the quasi-periodic time spectral method is that the period of motion must be known beforehand. If we examine the equations for the time spectral coefficients, equations (10), (11), (16), (17), etc., we see that the period of motion appears in each. For flutter problems, the flutter frequency is usually close to the natural frequency of pitch, but it is rarely exactly the same. Essentially, to solve the flutter problem using the BDFTS method, one needs to know the period of flutter, which is itself obtained by solving the flutter problem. To validate the BDFTS approach for aeroelastic problems we assume that period of flutter is known, in the present work (it can be found from the corresponding BDF2 solution). Ultimately, however, the period of flutter must be found as part of the BDFTS aeroelastic solution itself for this method to be viable for real world applications. Fortunately, Gopinath et. al.[19] has already demonstrated that it is possible to find the period of motion (in their case vortex shedding motion) while simultaneously solving for flow equations, although for a purely periodic problem. In furture work, a carefully picked objective will be used in conjunction with a similar, general strategy to find the period of flutter as the aeroelastic solution is found.

Finally, another drawback of the BDFTS aeroelastic approach is picking the number of time instances to use. When too few time insatnces are used for purely aerodynamic problems, the solution will converge, but will only include as many harmonics as the number of time instances allow, i.e. $\frac{N-1}{2}$ rounded down. However, even though most aeroelastic solutions appear to contain motion in only one harmonic, necessitating only three time instances, using three time instances has been found to yield inaccurate results or even to cause convergence failure. It has been found in the present work that a minimum of five time instances must be used. Ideally, we could use many (15 or more) time instances to guarantee accuracy and convergence, but the more time instances that are used, the longer the aerodynamic system takes to converge, so a desire exists to use as few time instances as possible.

III. Test Case and Results

A. BDFTS Aerodynamic Validation

The BDFTS method is validated for aerodynamic flow problems using the same test case as in our previous work:[10] a two-dimensional inviscid pitching-climbing motion using the NACA0012 airfoil. The test case Mach number is set to 0.555. A periodic pitching motion is prescribed about the airfoil's quarter chord. Simultaneously, the mean angle of attack of the airfoil changes as the airfoil translates with prescribed vertical and horizontal velocity transients. This motion is illustrated in Figure (2(a)), while the periodic pitching motion, mean angle of attack, and horizontal and vertical velocities of the airfoil are plotted in Figure (2(b)). The angle of attack is prescribed as:

$$\alpha(t) = \alpha_0 + \bar{\alpha}(t) + \alpha_1 sin(\omega_1 t) + \alpha_2 sin(\omega_2 t) \tag{40}$$

where the mean angle of attack is given as:

$$\bar{\alpha}(t) = \begin{cases} 0 & t < t_1 \\ \alpha_m \frac{1}{2}\{1 - cos[\omega_m(t - t_1)]\} & t \geq t_1 \end{cases}$$

where t_1 is the prescribed time at which the transient motion begins (taken as 1 period) and with the constants taken as:

$$\alpha_0 = 0.016^o, \quad \alpha_m = 2^o, \quad \alpha_1 = 2.51^o, \quad \alpha_2 = 1.25^o$$
$$\omega_1 = 0.1632, \quad \omega_2 = 3\omega_1, \quad \omega_m = 0.1\omega_1$$

The angle of attack and the forward/upward velocity are shown in Figure (2(b)), which clearly illustrates that the variations in the mean angle of attack and the airfoil translational motion represent slow transients compared to the periodic pitching motion, which itself contains multiple harmonics. Figure (3(a)) shows the comparison of the computed lift coefficient in the first period (based on the frequency ω_1). Because the highest mode of the pitching motion ω_2 is three times that of the base mode ω_1, seven time instances are need to produce an accurate solution. Also, from Figure (3), the BDFTS scheme with five time instances shows poor agreement with the reference BDF2 results obtained using 512 time steps per period. On the other hand, using seven or more time instances with the BDFTS scheme produces very good agreement with the reference BDF2 solution over the complete time history which includes eleven periods, as shown in Figure (3(b)).

B. BDFTS Structural Validation

The solver for the structural equations discretized in the BDFTS framework is validated independently of the flow solver. Lift (C_L) and moment (C_m) coefficents are prescribed as functions of time and the structural equations given by (38) and (39) are solved for the time-implicit and time-spectral frameworks, respectively. For the time-implcit case, the $[4x4]$ structural matrix is directly inverted for each time-step. For the time-spectral case, the $[(4xN)x(4xN)]$ structural matrix is inverted using a simple GMRES algorithm. Note that N in the BDFTS matrix is the number of time instances used.

As long as a sufficient number of time steps are used in the BDF2 approach and a sufficient number of time-spectral instances N are used to account for the harmonics present in the prescribed lift and moment coefficient functions for the BDFTS approach, agreement between BDF2 and BDFTS is exact (to computational accuracy) for the structural equations alone.

C. Aeroelastic Validation

To validate the aeroelastic aspect of the solvers the two-dimensional swept wing model exhibiting the transonic dip phenomenon suggested by Isogai[20] is chosen as the test case. The structural parameters for this case are:

x_α = 1.8
r_α^2 = 3.48
$\frac{\omega_h}{\omega_\alpha}$ = 1.0
μ = 60
a = -2.0

The quantity a is the non-dimensional elastic axis location along the chord of the airfoil measured from the mid-chord of the airfoil when it is in the neutral position. Since it is non-dimensionalized by the semi-chord of the airfoil, the elastic axis is located half a chord length ahead of the leading edge of the airfoil in this particular case. The airfoil under consideration is the NACA64a010 (Ames) airfoil operating with a mean angle-of-attack α_0 of 0^o and an amplitude of forced pitching α_{max} of 1^o. A computational mesh composed of 1717 nodes and 3280 elements is used, as shown in Figure (4). For the BDF2 time implementation, the solution process involves forcing the airfoil in pitch for three periods at the natural frequency of pitch before allowing it to respond aeroelastically. Between 64 and 128 timesteps per period were used for these calculations depending on the length of the period. The convergence of the first few timesteps of a BDF2 solution are shown in Figure (5). The goal of the validation procedure is to compute and compare a flutter boundary against existing data. Computation of the flutter boundary is performed by manually modifying the flutter velocity at various Mach numbers with the objective of obtaining a neutral aeroelastic response. Although the aeroelastic solvers were not directly validated against experimental data, the predicted flutter boundary

matches well with computational results from References[13,15] as indicated by the flutter diagram in Figure (6). The flow solution at two different time-steps is shown in Figure (7) for a flutter case at $M_\infty = 0.875$. This plot show how the shockwaves transverse the airfoil with its flutter motion.

D. BDFTS Aeroelastic Results

The BDFTS flow solver, validated above, is combined with the aeroelastic structural equations discretized according the BDFTS approach to form a BDFTS aeroelastic solver. The solution process for the BDFTS implementation is as follows: first a purely periodic time spectral solution is found at the flutter frequency. Then, a single period of first-order BDFTS is solved as the airfoil is allowed to respond aeroelastically. Next, enough additional periods are run using second-order BDFTS to determine if the solution is aeroelastically damped, neutral, or excited (i.e. experiencing flutter). It should be noted that for now, the period of flutter is assumed to be known and prescribed for the BDFTS solutions.

A damped, neutral, and excited case are run using the same structural parameters and computational mesh as in subsection (III.C) above. Figures (8)-(10) compare BDFTS flutter solutions to the corresponding time-implicit solution. It should be noted that the BDF2 solutions were rerun using the flutter frequency for the first three prescribed periods to facilitate direct comparison of the data. As can be seen from these figures, there is close agreement between the time-implicit and time-spectral solutions, indicating that the BDFTS method is capable of solving the coupled fluid/structure equations. Most importantly, the solutions exhibit the correct flutter response, i.e. damped, neutral, or excited. The cases presented in Figures (8)-(10) were all run at a free stream Mach number $M_\infty = 0.875$, using five time-spectral instances, and at the flutter velocity indicated by the Figure caption. It should also be noted that, although BDFTS and BDF2 response plots match almost exactly for the neutral response, the BDFTS response decays more slowly in the damped case and grows more slowly in the excited case. This discrepency is thought to result from the BDFTS aeroelstic coupling and will be investigated further in future work.

Figure (11) shows the convergence of the BDFTS aeroelastic solver. Figure (11(a)) demonstrates that the FGMRES flow solver converges the flow equations quadratically. Figure (11(b)) shows this same period of prescribed motion (ending at interation 180), plus the first two aeroelastic response periods (the first of which ends at iteration 675). Each of the short dips in these two aeroelastic periods indicates that the mesh was moved to accomodate updated structural variables. The flow solver converges to machine zero in only two to three non-linear iterations for each update of the structure. The noteworthy trend in which the flow residual returns to a smaller value each time the structure is moved indicates the structure is being moved less with each subsequent update; in other words, the fully-coupled aeroelastic problem is converging for all time instances.

Although good agreement was reached for the above cases, many other cases on the flutter boundary diagram given in Figure (6) eluded solution. Specifically, these cases would diverge as the coupling procedure given in subsection (II.B.3) was repeated. Generally, cases with a flutter velocity above $V_f > 0.7$ could not be solved at present. It is thought that these difficulties result from inadequate coupling between the two sets of equations. To remedy this problem, a stronger coupling strategy must be produced.

IV. Conclusions and Future Work

The BDFTS method has been demonstrated to be capable of solving the coupled unsteady fluid-structure equations and results compare favorably with the standard time-implicit solutions. However, further improvements are needed in order for this method to solve flutter problems efficiently and without any prior knowledge about the airfoil response characteristics. First, a method must be found to allow for the resolution of the flutter period as the BDFTS aeroelastic solution progresses. Next, a method to couple more strongly the fluid and structure equations must be devised. Finally, the general solver efficiency needs to be improved so that many time instances can be used without concern for degredation of the solution speed. We also anticipate that this method can be extended to gust response and other quasi-periodic, coupled fluid/structure problems in the future.

References

[1]Hall, K. C., Thomas, J. P., and Clark, W. S., "Computation of Unsteady Nonlinear Flows in Cascades Using a Harmonic Balance Technique," *AIAA Journal*, Vol. 40, No. 5, 2002, pp. 879–886.

[2]McMullen, M., Jameson, A., and Alonso, J. J., "Acceleration of Convergence to a Periodic Steady State in Turbomachineary Flows," AIAA Paper 2001-0152, Jan. 2001.

[3]McMullen, M., Jameson, A., and Alonso, J. J., "Application of a Non-Linear Frequency Domain Solver to the Euler and Navier-Stokes Equations," AIAA Paper 2002-0120, Jan. 2002.

[4]Gopinath, A. K. and Jameson, A., "Time Spectral Method for Periodic Unsteady Computations over Two- and Three- Dimensional Bodies," AIAA Paper 2005-1220, Jan. 2005.

[5]van der Weide, E., Gopinath, A. K., and Jameson, A., "Turbomachineary Applications with the Time Spectral Method," AIAA Paper 2005-4905, June 2005.

[6]Lee, K.-H., Alonso, J. J., and van der Weide, E., "Mesh Adaptation Criteria for Unsteady Periodic Flows Using a Discrete Adjoint Time-Spectral Formulation," AIAA paper 2006-0692, Jan. 2006.

[7]Sankaran, S., Gopinath, A., Weide, E. V. D., Tomlin, C., and Jameson, A., "Aerodynamics and Flight Control of Flapping Wing Flight Vehicles: A Preliminary Computational Study," AIAA 2005-0841, Jan. 2005.

[8]Choi, S., Potsdam, M., Lee, K., Iaccarino, G., and Alonso, J. J., "Helicopter Rotor Design Using a Time-Spectral and Adjoint-Based Method," AIAA 2008-5810, Sep. 2008.

[9]Choi, S. and Datta, A., "CFD Prediction of Rotor Loads using Time-Spectral Method and Exact Fluid-Structure Interface," AIAA 2008-7325, Aug. 2008.

[10]Yang, Z. and Mavriplis, D. J., "Time spectral method for quasi-periodic unsteady computation on unstructured meshes." AIAA Paper 2010-5034, June 2010.

[11]Yang, Z., Mavriplis, D. J., and Sitaraman, J., "Prediction of Helicopter Maneuver Loads Using BDF/Time Spectral Method on Unstructured Meshes," AIAA Paper 2011-1122, June 2011.

[12]Mavriplis, D. J., Yang, Z., and Mundis, N. L., "Extensions of Time Spectral Methods for Practical Rotorcraft Problems," AIAA paper 2012-0423, January 2012.

[13]Alonso, J. J. and Jameson, A., "Fully-Implicit Time-Marching Aeroelastic Solutions," AIAA paper 1994-0056, Jan. 1994.

[14]Mani, K. and Mavriplis, D. J., "Linearization of the Coupled Unstead Fluid-Structure Equations: Application to Flutter Control," AIAA paper 2008-6242, August 2008.

[15]Willcox, K. and Peraire, J., "Aeroelastic computations in the time domain using unstructured meshes," *International Journal for Numerical Methods in Engineering*, Vol. 40-13, 1997.

[16]Canuto, C., Hussaini, M. Y., Quarteroni, A., and Zang, T. A., *Spectral Methods in Fluid Dynamics*, Springer, 1987.

[17]Hesthaven, J., Gottlieb, S., and Gottlieb, D., *Spectral Methods for Time-Dependent Problems*, Cambridge Monographs on Applied and Computational Mathematics, 2007.

[18]Gottlieb, D. and Orszag, S. A., "Numerical Analysis of Spectral Methods: Theory and Applications," CBMS-26, Regional Conference Series in Applied Mathematics, SIAM,Philadelphia, PA, 1977.

[19]Gopinath, A. K. and Jameson, A., "Application of the Time Spectral Method to Periodic Unsteady Vortex Shedding," AIAA Paper 2006-0449, Jan. 2005.

[20]Isogai, K., "Transonic Dip Mechanism of Flutter of a Sweptback Wing: Part II," *AIAA Journal*, Vol. 17, 1981, pp. 1240–1242.

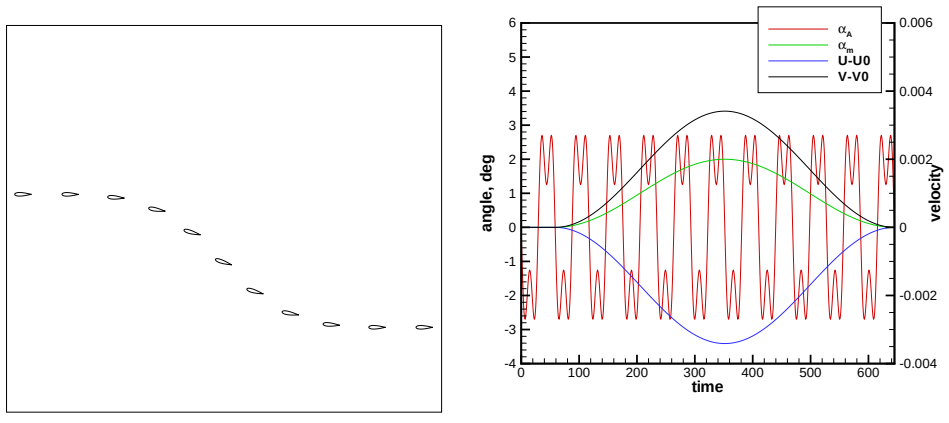

(a) (b)

Figure 2. (a) Illustration of quasi-periodic pitching-climbing airfoil and (b) prescribed horizontal and vertical velocities and pitching angle.

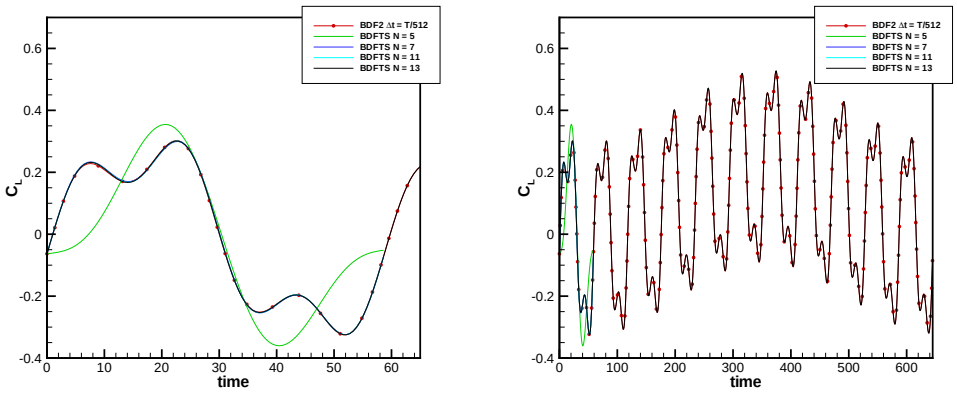

Figure 3. Comparison of computed lift coefficient using BDFTS versus time-domain (BDF2) solution for (a) first period of motion and (b) 11 periods of motion for pitching-climbing airfoil.

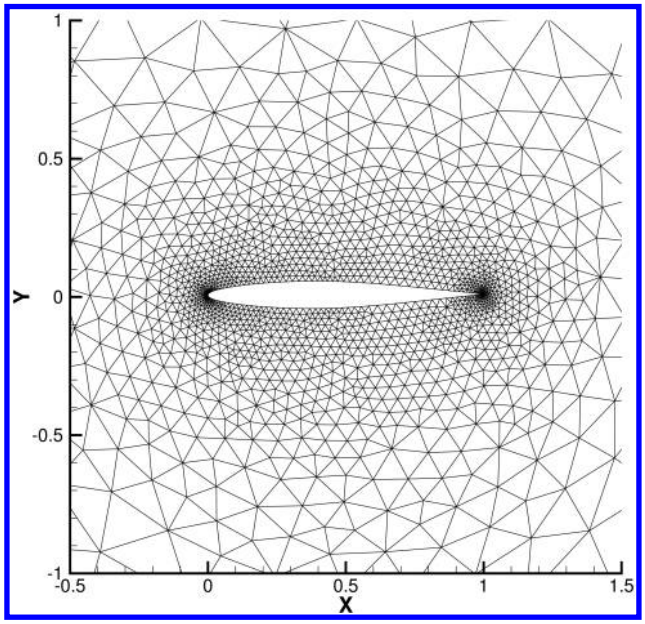

Figure 4. Nearbody computational mesh for the NACA64a010 airfoil (1717 nodes, 3280 elements)

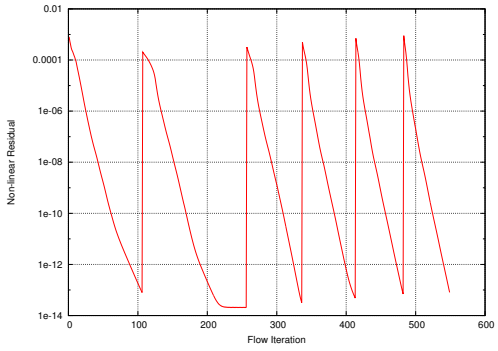

Figure 5. Convergence of the BDF2 flow solver for the first six time-steps

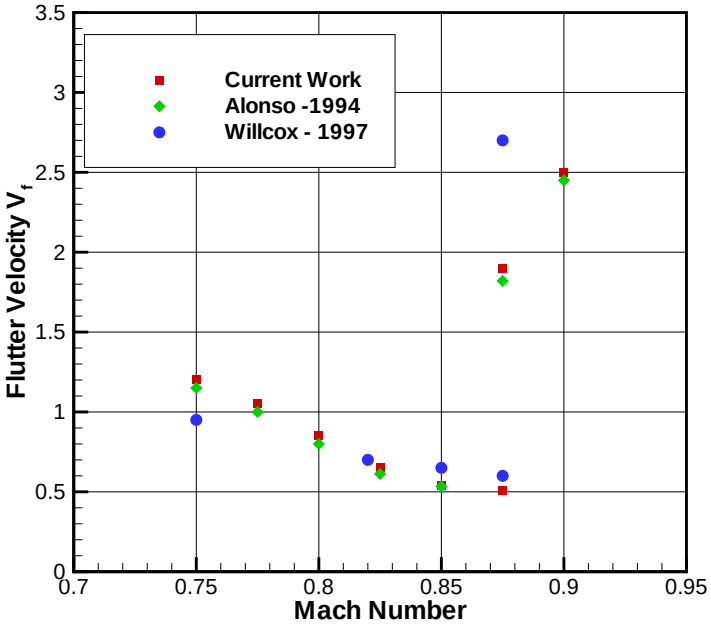

Figure 6. Comparison of predicted flutter boundary against other references

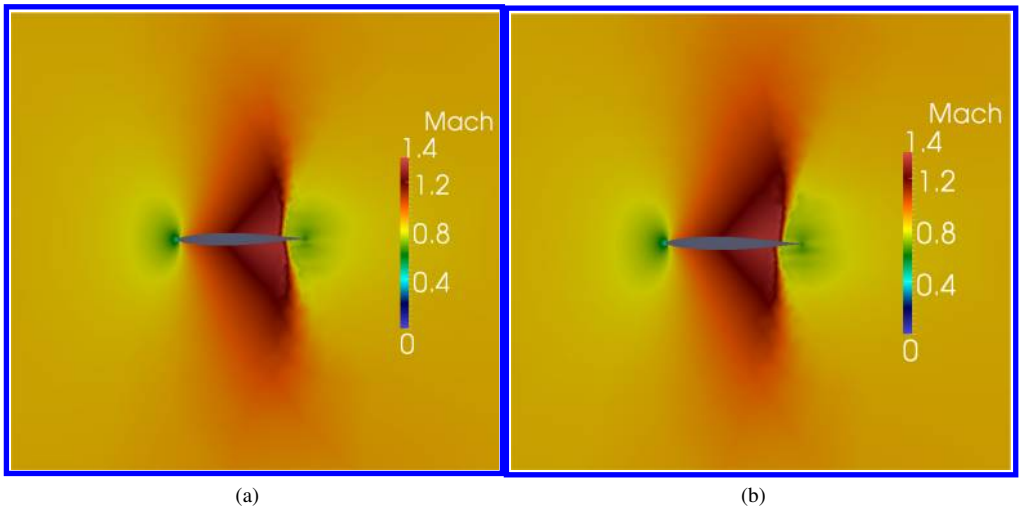

(a) (b)

Figure 7. Flow solutions for $M_\infty = 0.875$ demonstrating the change in position of the shockwave with airfoil orientation

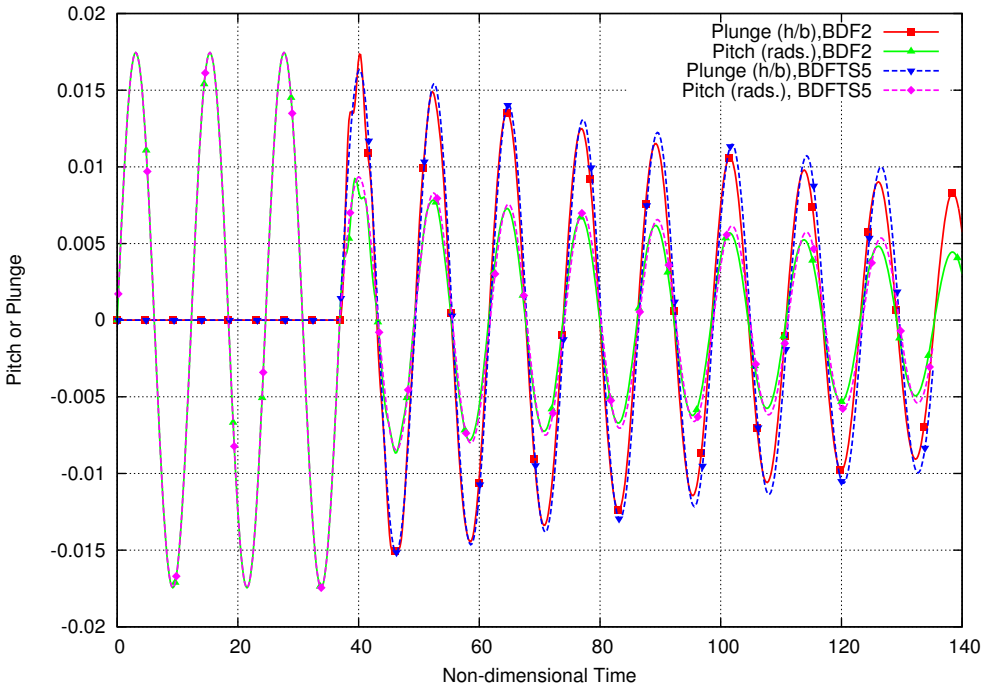

Figure 8. Comparison of the Aeroelastic response for BDF2 and BDFTS methods: Damped response ($M_\infty = 0.875, V_f = 0.4$)

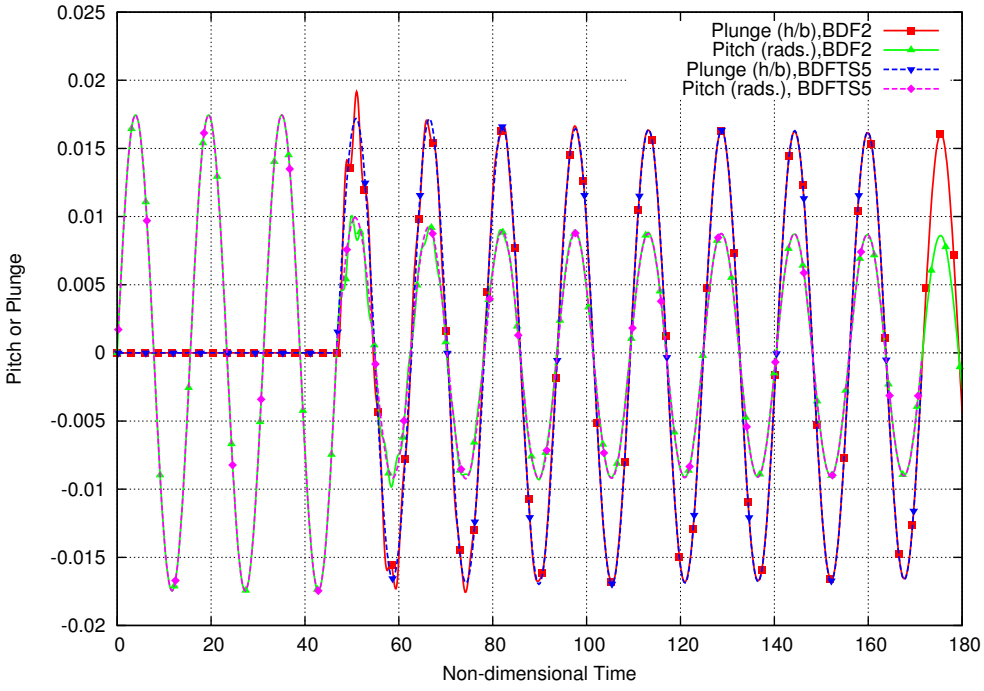

Figure 9. Comparison of the Aeroelastic response for BDF2 and BDFTS methods: Neutral response ($M_\infty = 0.875, V_f = 0.537$)

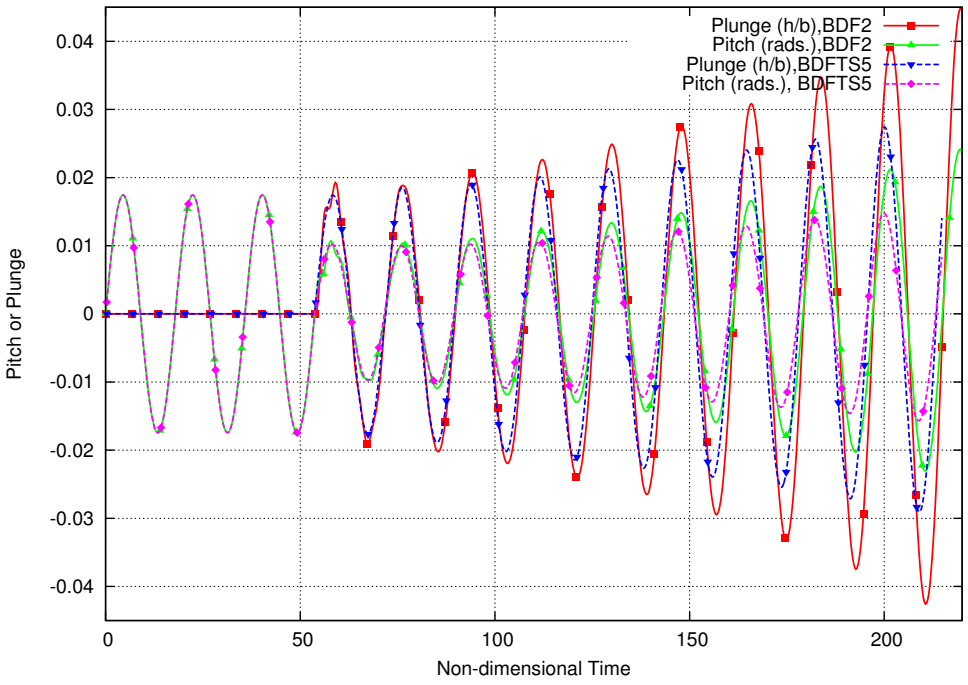

Figure 10. Comparison of the Aeroelastic response for BDF2 and BDFTS methods: Excited response ($M_\infty = 0.875, V_f = 0.65$)

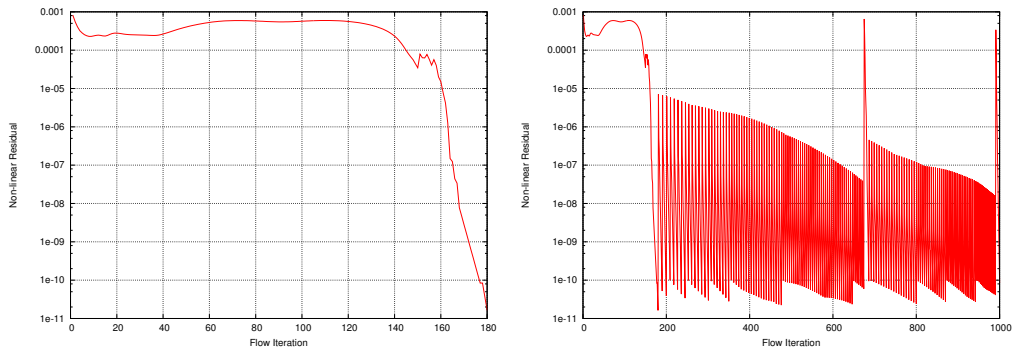

(a) (b)

Figure 11. BDFTS flow convergence for (a) the initial, prescribed motion; and (b) the inital motion plus the first two periods of aeroelastic response